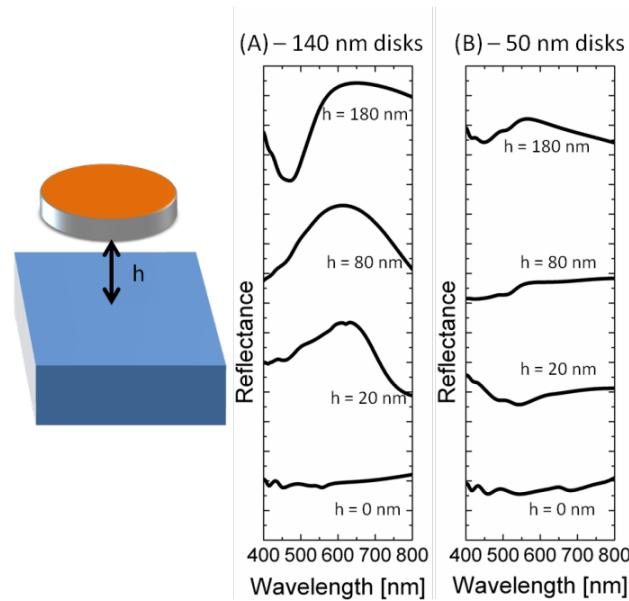# Printing Colour at the Optical Diffraction Limit

Karthik Kumar[1,#], Huigao Duan[1,#], Ravi S. Hegde[2], Samuel C.W. Koh[1], Jennifer N. Wei[1]

*and*

Joel K.W. Yang[1] *

Figure S1. Simulated reflectance spectra of nanodisks in the presence of Si in vacuum

Figure S1. Simulated spectra of Ag/Au nanodisks hovering above a reflective Si surface. The spectra for both (A) 140 nm disks and (B) 50 nm disks in periodic arrays with gaps of 30 nm are presented here. When the disks are placed directly on a reflective surface (0 nm), all visible wavelengths appear to be reflected almost equally, which would result in a dull gray colour. As soon as the nanodisks are allowed to hover above the surface even at a distance of 20 nm, the spectrum shifts drastically; plasmonic scattering is observed for the larger nanodisks, while certain wavelengths are absorbed of the smaller nanodisks. At a distance of 180 nm, more of the low wavelength regions are reflected, resulting in a bluish tinge to the colours observed.
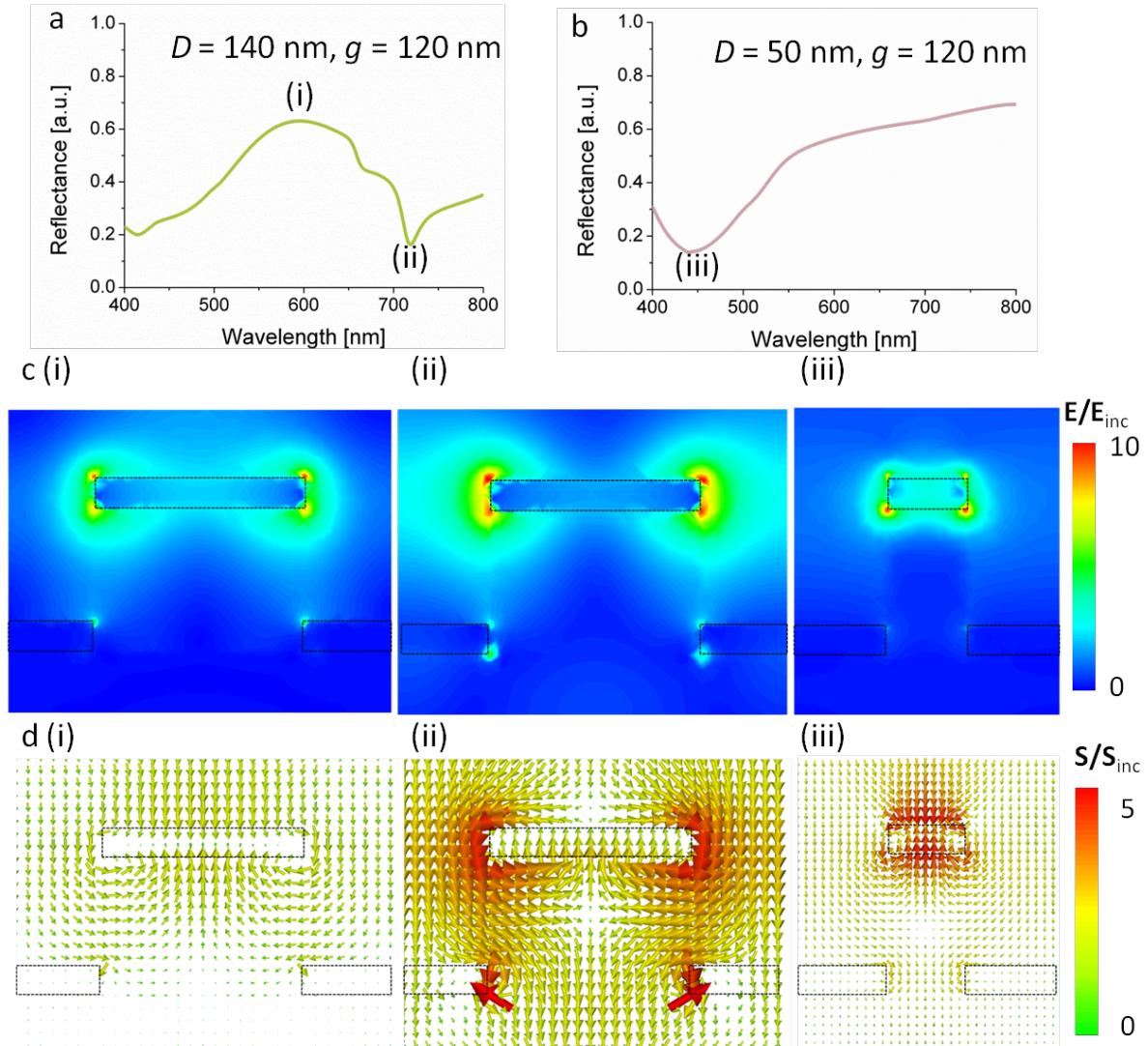
The behavior of nanodisks in the vicinity of a back-reflector can be explained via the existence of a screening dipole, which is a mirror dipole, and thus has the opposite effect the orginal dipole. The dipoles are thus cancelled out. The cancellation is most effective when the dipoles are closest to each other. Thus when resting right on top, there is almost full cancellation and as we start hovering the disk, the cancellation becomes less effective. The role of the HSQ structures can thus be hypothesized to be due to the reduction of the effects of the screening charges.[1,2] It is highly likely that once the nanodisks are separated far enough from the surface, the configuration of nanodisk and reflective surface will produce a superposed response of the individual spectra from the nanodisk and the silicon surface.

Figure S2. Experimental Microspectrophotometry Data
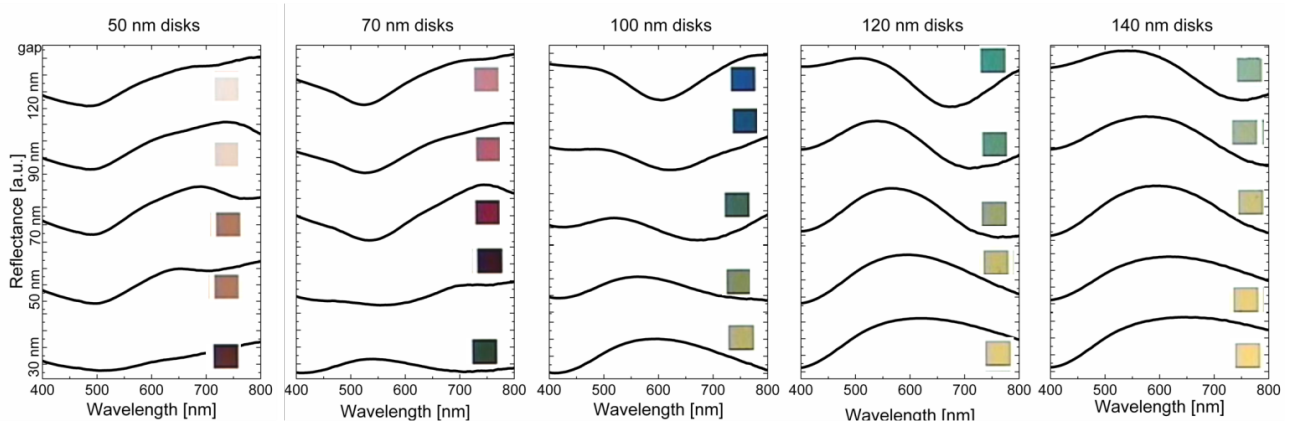
Figure S2. Selected experimentally obtained spectra with varying *D* and *g*. The corresponding colours observed in reflection brightfield microscopy are also displayed.

Figure S3. Simulation results, electric field and Poynting vector plots for an array of nanopillar structures with separations of 120 nm. (a) 140 nm disks: A peak at 590 nm (i) and a dip at 710 nm (ii) are observed. The corresponding E-field amplitude enhancement plot (ci) shows that a dipole resonance is present in the disk at this point, while the Poynting vector plot (di) shows that most of the power is reflected away towards the observer. At the dip at 710 nm, the corresponding E-field plot (cii) shows a strong

5

resonance within the disk, while the Poynting vector plot (dii) shows how the power flows around the nanodisk into the nanohole. (b) 50 nm disks: A single dip at 440 nm (iii) is observed. The corresponding E-field plot (ciii) shows that a strong dipole resonance is set up within the nanodisk, while the Poynting vector plot (diii) shows how the power flows mostly into the nanodisk and towards the nanohole.

To investigate the observed spectral features in the reflectance plots, we looked at the simulated electric field amplitude enhancement (E-field) plots and Poynting vector plots at the peaks and dips for 140 and 50 nm disks (Figures S3a and S3b, reproduced for clarity from Figure 2cii). Two key features for disks with a diameter of 140 nm (Figure S3a), i.e. a clear peak at ~590 nm, and a dip at ~710 nm are observable. At the peak, we see strong E-fields around the disk (Figure S3c(i)) and Poynting vector plots (Figure S3d(i)) showing energy flow *into* the disk, both signifying the condition of a disk plasmon resonance, which re-radiates light back to the viewer.[3] On the other hand, at the dip (~710 nm), we observe both a strong E-field (Figure S3c(ii)) *around* the disk and through the hole of the back-reflector. The Poynting vector plot (Figure S3d(ii)) shows that power is being channeled sharply around the disk and into the hole. Hence, the peak of reflectance occurs at the plasmon resonance of the disk, whereas the dip in reflectance corresponds to the antenna-assisted EOT mode.

As the disk size is reduced to between 90 nm to 50 nm, we note the disappearance of the peak, and a blue-shifting in the position of the dip (Figures 2c(ii), S3b). Observing the field plots (Figure S3c(iii)) and Poynting vector plots (Figure S3d(iii)) at this dip at

~440 nm, we see the strong E-fields around the disk and energy being channeled *into* the

disk and hole suggesting the behavior of the nanostructures as an anti-reflection stack.

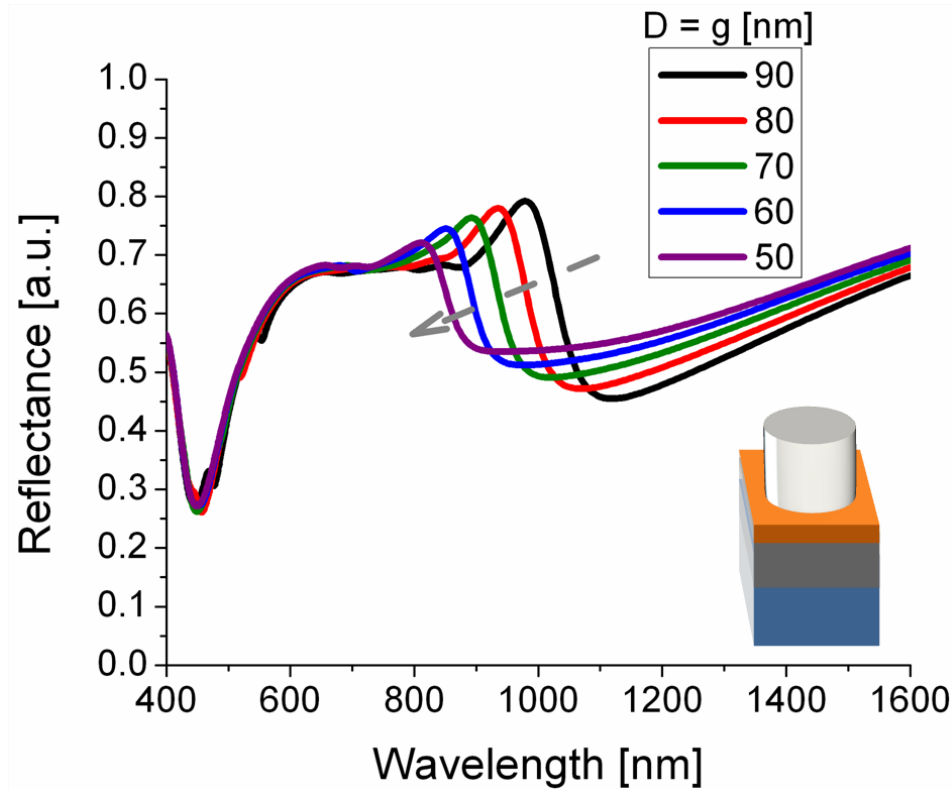**Figure S4. Simulated reflectance spectra of nanodisks in vacuum**
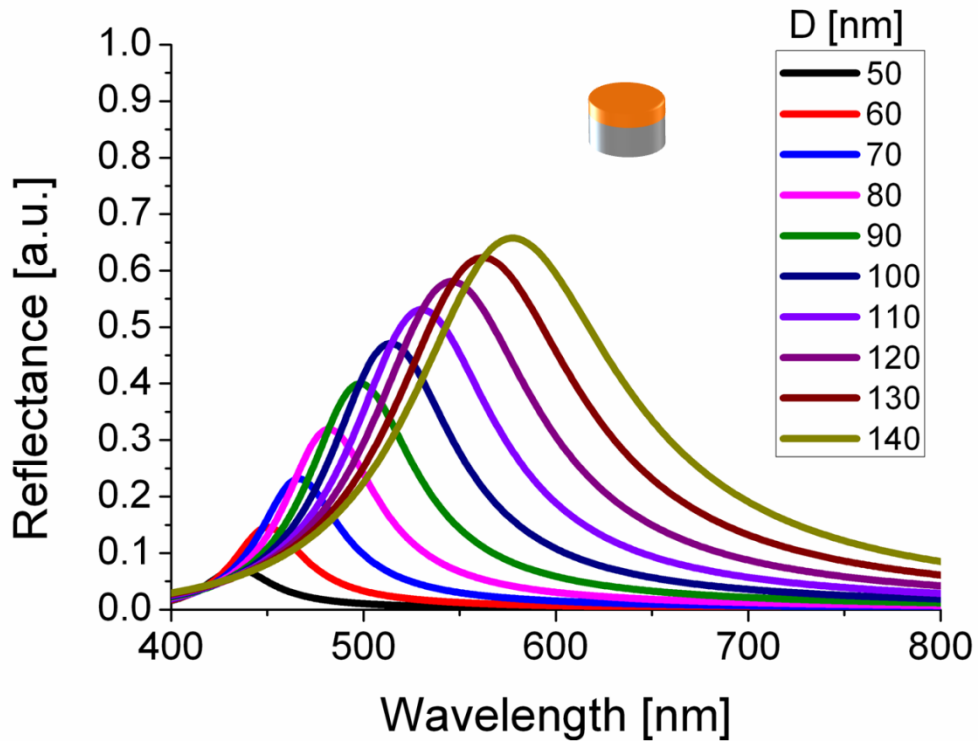
Figure S4. Simulation of the reflectances of an array of disks with a separation of 120 nm in vacuum. The peak position of the reflectance red-shifts from 430 nm to 580 nm with increasing diameters of the nanodisk. The reflectance intensity also increases with increasing diameter of the nanodisks.

Figure S5. Simulation of the reflectances of an array of nanoholes in an Ag/Au stack. The fill factor is kept constant at 0.5 [$D/(D+g)$] with the diameter and the gap being equal to each other. EOT modes are detected for these cases which redshifts from 850 nm to 1050 nm with increase in periodicity as indicated by the gray arrow. The dip position of the reflectance stays fairly constant at ~ 450 nm, indicating that the absorbance at this region is independent of periodicity. This dip may be attributed to the anti-reflection coating stack of Au/Ag on Si at this wavelength.

**Figure S6: Effect of holes at the base of the nanoposts in the backplane**
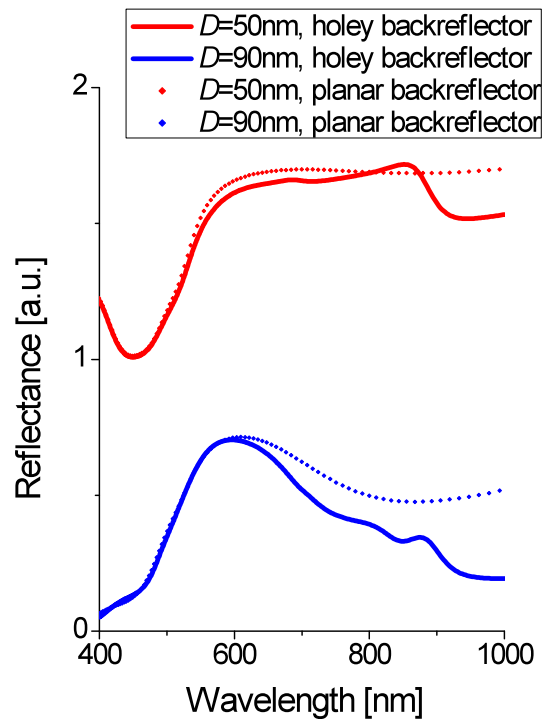
Figure S6. Numerical simulations of the structures with and without the presence of a hole in the backreflector plane. The periodicity was kept constant at 120 nm and simulations were done for the cases of $D = 50$ nm and 90 nm to compare with those in Figure 3. The inflexion points at 900 nm disappear for the case of the planar backreflector, due to the absence of Fano resonances. For $D = 90$ nm, the nanoholes reduce reflectance in the red part of the spectrum and at longer wavelengths thus accentuating the blue and green colors.

<u>Figures S7 and S8: Layout Generation</u>

Red, green, and blue (RGB) values for each combination of disk size (*D*), and gap size (*g*) were first extracted from the optical micrograph of the colour palette of Figure 2(b), as presented in Figure S7. A code was written in Matlab to generate pattern layouts for the electron-beam lithography tool based on a bitmap image. The code then extracts RGB values for each pixel and finds a closest match to a combination of *D* and *g* from the colour palette using a least-squares error method. Each pixel was defined to occupy an area, which could be set to an arbitrary value, e.g. 250 nm by 250 nm square (as presented in the main text). To fit disks into this pixel array, two approaches were used. The first, which was used to create the bowtie image (Figure S7a-c) simply used the exact *D* and *g* obtained from the closest match and fitted a 2x2 array of disks into the square area. The 2x2 array would fit inside this square array if the condition $2*(D+g) < 250$ nm was satisfied, but if a situation arose such that $2*(D+g) > 250$ nm, only a single disk of size *D* was positioned at the center of the square. This approach could lead to inaccuracies in the colour reproduction.

In the second approach, used in the main text, we make use of the fact that lines of almost equal colour exists on the *D* vs *g* plot. This approach was used to create the Lena image (Figure 4a-c). It would first find the closest match for *D* and *g* just like the first method, but would then scale *D* and *g* to *D'* and *g'* along lines of nearly equal colours on the *D* vs *g* plot. These lines were approximately defined to be lines of equal slopes such that $(D'-D)/(g'-g) = ½$, which should also satisfy the equation $2*(D'+g') = 250$ nm. The resulting disks would be a periodic array of disks with varying *D'* and *g'* values. In

11

cases where a single disk would suffice, e.g. in the rendering of blue/purple colour in the Lena image, the code would decide this by comparing the fractional change in D' and g' for both cases to the original D and g and choosing the case with the smaller fractional change. The code would then create an entry in the layout file for the coordinates of these 4 disks within the pixel area. Further improvements in the code can be obtained by including the ability of colour prediction, interpolating between data points, and by feeding in more data points for a larger range of D and g values.
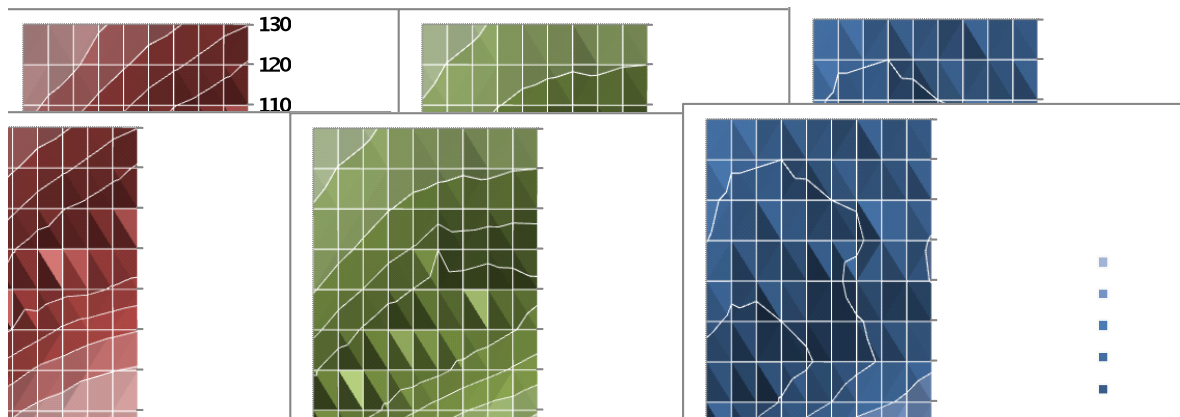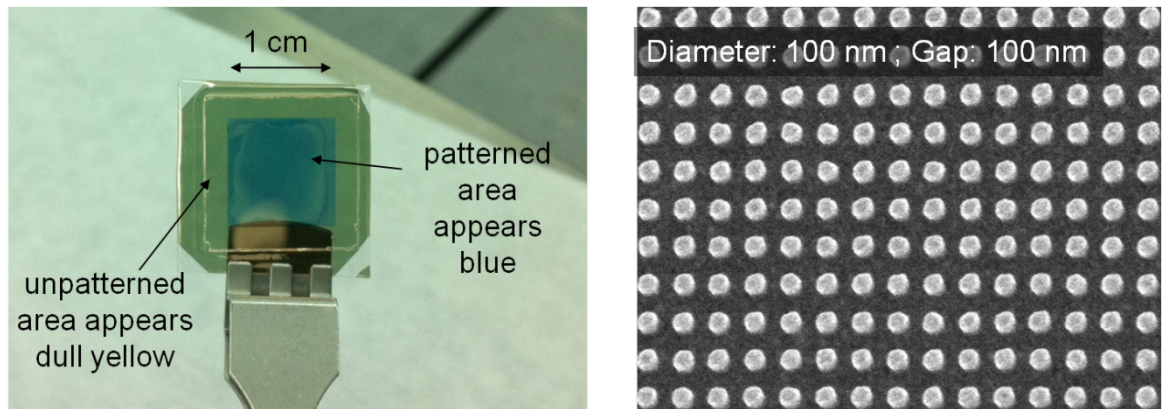

Figure S7. Plots of R, G, and B values on a D vs g axis extracted from the optical micrograph of the colour palette in Figure 2(b). These RGB values with their corresponding D and g combinations were used by the code to find a closest colour match for every pixel in a given bitmap image. The closest match for D and g, or modified D' and g' values were then used to calculate the coordinates and sizes of each disk in the layout.

12
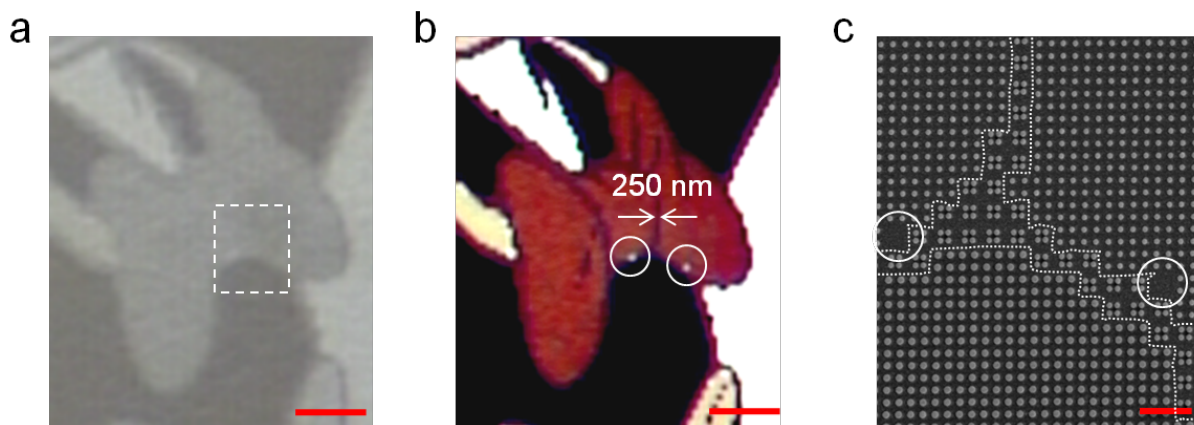
Figure S8: Arbitrary full-colour image printing. (a) A colour image prior to deposition of the metal layers, the optical micrograph shows at best grayscale variations (cf. Figure 2a). (b) Upon deposition of the uniform metal layers, the various solid colours emerge. (c) SEM image of a selected area in 4a, showing the structures' array, with the exact two bright dots that appear in 4b as circled. Dotted lines were drawn in to show boundaries between the different colors.

Figure S9. Photograph and SEM images showing results obtained with nanoimprint lithography. To investigate the feasibility of scaling-up the throughput of such plasmonic micro-images, we used thermal nanoimprint lithography to create a 1 x 1 cm area of nanopillars in polycarbonate (see Methods section). The nanopillars were subsequently coated with a metal layer. The patterned areas had a blue colour, while the unpatterned areas retained the bulk metal layer colour.

14

1   Dimitriev, A. *et al.* Enhanced nanoplasmonic optical sensors with reduced substrate effect. *Nano Lett.* **8**, 3893-3898 (2008).

2   Zhang, S., Bao, K., Halas, N.J., Xu, H. & Nordlander, P. Substrate-induced fano resonances of a plasmonic nanocube: A route to increased-sensitivity localized surface plasmon resonance sensors revealed. *Nano Lett.* **11**, 1657-1663 (2011).

3   Liu, N. *et al.* Plasmonic analogue of electromagnetically induced transparency at the drude damping limit. *Nature Mater.* **8**, 758-762 (2009).